ESI Preprints **Not Peer-reviewed**

Landslide Soil Failure Parameters Characterization Using Geoelectrical Resistivity Methods in Uruagu, Nnewi, Anambra State, Nigeria

Charles Chinedu Uwaezuoke
Osariere John Airen
Department of Physics, University of Benin, Benin City, Nigeria.

Doi: 10.19044/esipreprint.2.2023.p116

Approved: 04 February 2023
Posted: 09 February 2023

Cite As:
Uwaezuoke C.C. & Airen O.J.(2023). *Landslide Soil Failure Parameters Characterization Using Geoelectrical Resistivity Methods in Uruagu, Nnewi, Anambra State, Nigeria.* ESI Preprints.
https://doi.org/10.19044/esipreprint.2.2023.p116

Abstract

Electrical Resistivity Imaging (ERI) and Vertical Electrical Sounding (VES) were deployed over Uruagu landslide area. The main purpose of the geoelectrical resistivity surveys was to characterize the landslide failure parameters in order to identify the soil failure mechanisms.

Ten profiles of 2D Electrical Resistivity Imaging (ERI) measuring 200 m each, and thirty Vertical Electrical Sounding (VES), with three VES along each profile, were executed. Nine of the ten profiles were executed within the landslide site while one profile was executed in a residential street as a control profile. Four soil samples were also taken for physical and geotechnical laboratory index analysis. The PASI resistivity meter was used for the geoelectrical resistivity measurements. The Wenner-Schlumberger array was deployed for the ERI with a minimum electrode spacing of 10 m. The Schlumberger array was deployed for the VES with a maximum current spacing of 130 m. ERI resistivity data analysis involved inversion using RES2DINV software package involving mean model residual and construction of iso-apparent resistivity contour maps. VES resistivity data analysis involved calculated parameters from plotted field data on log-log graph then used as initial models in an iterative forward modeling WinResist software package.

The results of the ERI and VES for the control profile reveal that the subsurface strata are originally composed of silty clay of resistivity values (16.7 – 60.9) Ωm, clayey silty sand having resistivity values (116 – 800) Ωm and sandstone layer with resistivity values (>814 Ωm). The ERI and VES results for the devastated landslide site reveal counteraction material of resistivity values (>814 Ωm), colluvia and regoliths (116 - 300 Ωm) and variably wet weathered sandstones of resistivity values (<60.9 Ωm). The laboratory results revealed the landslide site is majorly composed of silty sandy clay, silty clay, sandy silty clay and sandstones as the pre-landslide existing lithologies. The natural water content ranges from 10.6% to 14.0%. The liquid limit ranges from 44.0% to 46.0%, the plastic limit ranges from 15.0% to 17.0% and the plasticity index from 28.0% to 29.1%.
The geophysical and laboratory results revealed consistency in the lithological units in agreement to the characteristic geology of the study area. The landslide site has high gully slope gradients and collects large volume of floods during intense rainy season. These soils during intense rainfall, imbibe more water, following their high plasticity, slid along the sandstone to activate the soil failure.

Keywords: Landslide, Electrical Resistivity, Electrical Sounding, geoelectrical, Wenner-Schlumberger, laboratory index analysis

1.0 Introduction

Changes in stability conditions of the near-surface earth materials can lead to some natural phenomena like landslides, subsidence, groundwater vulnerability and other environmental geo-hazards.

Landslides are the movement of a mass of rock, debris or earth material down a slope under the influence of gravity; they are complex, strongly heterogeneous natural phenomena triggered by a variety of external factors, such as intense rainfall, earthquake shaking, water level changes and rapid stream erosion that cause a sudden change in shear strength of slope-forming materials. More so, to these causes, are human activities, such as excavation of slopes for road cuts into unstable hill-slope areas, (Bogoslovsky and Ogilvy, 1977; Yilmaz, 2011; Merritt *et al*., 2013). Landslide types exist in different regions of the world, showing varying states, distributions and styles of activity and are predominant in areas where clayey formations are common in deposits (Cruden and Varnes, 1996;). Landslide in Uruagu community of Nnewi North in Anambra State, Nigeria, has wrecked damages worth several millions of dollars in monetary losses, and are responsible for thousands of deaths and injuries annually, (Igwe and Una, 2019). Landslide mechanisms, impacts and management are often determined by the geology, hydrogeology and geomorphology of the area

(Igwe and Una, 2019). Therefore, landslide characterization demands some extensive non-discrete investigational survey.

In recent times, successful geoelectrical resistivity methods of geophysical investigations, as reported in literature, have proven most resourceful in the characterization of sites for landslide, groundwater and a host of other engineering, hydrogeological, geomorphological and environmental investigations (McCann and Foster, 1990; Daily and Ramirez, 2000; Loke, 2001; Dahlin et al., 2006; Drahor et al. 2006; Schrott and Sass, 2008; Ayolabi et al., 2013; Sechman et al 2013; Egbueri and Igwe, 2018; Pazzi et al. 2019; Uwaezuoke et al. 2021).

Arising from the daily increase in population, urbanization drive and quest in more land usage in Uruagu Nnewi metropolis, the landslide menace will lead to more retardation in developments and socioeconomic devastation. In response to this menace, this study was aimed at characterising the landslide failure parameters using geoelectrical resistivity methods in order to identify the soil failure mechanisms. The objectives were: (i) to measure the geoelectrical resistivity, determine the textural and index test properties of soil/rock samples from laboratory analysis of the study areas (ii) to delineate the subsurface lithology of the study area into its geologic layers from the measured geophysical properties (iii) to determine the depth of the landslide slip surface, hydrogeological and strength parameters of the geologic structures (iv) to deduce environmental and engineering projections to non-landslide zones.

1.1 Location, Physiography and Geology of the Study Area

The study area (Figure 1), Uruagu landslide site, is located in Nnewi metropolis/ Nnewi North in Anambra State, southeastern Nigeria. Nnewi North L.G.A is boundary-circled by Idemili South, Nnewi South and Ekwusiogo local government areas. It is located between latitude N6°.00'and N6°.04' and Longitude E6°.54' and, E6°.57'.

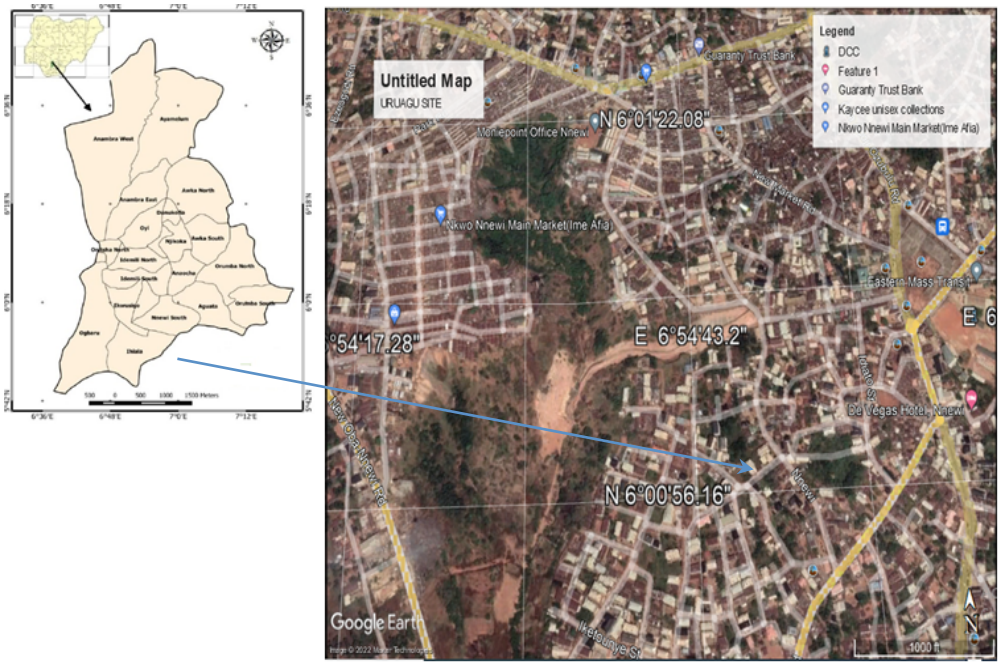

Figure 1. Location of the Study Area

The study site is an active landslide location involving slide, fall and flow of debris and colluvia. A drainage channel of large expanse for flood runs within the site. The landslide is usually initiated and reactivated within hours of intense rainfall during the rainy seasons, with buildings lost over the years, localities displaced and threatening to cut off the adjoining major public roads. The topography is steeply sloppy concave terrain with elevations ranging from 111 m to 142 m (Figure 2) indicative of washed away in-situ soils/lithology.

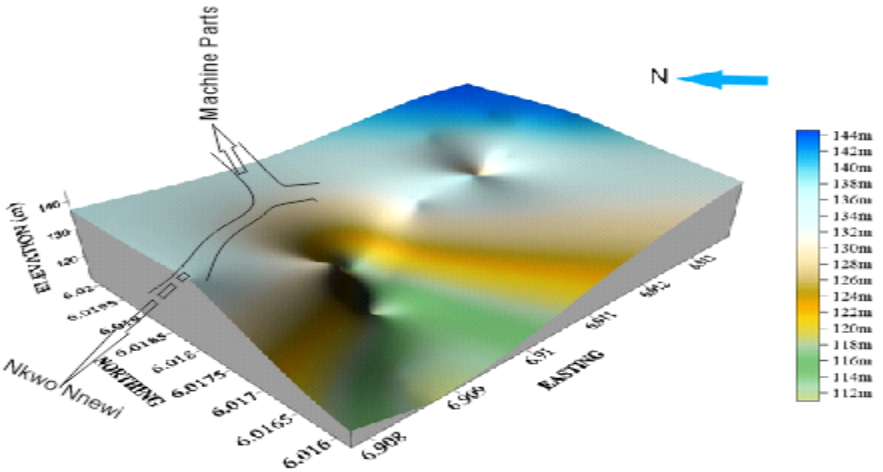

Figure 2. Site Topography

Endangered abandoned buildings with cracks are located on the crown flanks of the site. Recently, the state government did some remediation and counteraction works on the concave dips towards the major road network in order to halt the landslide advancement. The counteraction works involved rocks embankments, granite boulders, soils covering of various types. Fractured bedrock sandstones are visibly exposed at the slopy end of the site. The climatic condition is moderately hot and humid associated with southeastern Nigeria. There are two distinct seasons in the state, namely, the rainy season which lasts from March/April to October/ November and the dry season which lasts for the rest of the year, October/November till March/April. The distribution of rainfall varies annually between 1500 mm to 2500 mm (Monanu and Inyang 1975; NIMET, 2007; Ezemonye and Emeribe 2012 and Igwe et al. 2013). The average monthly temperatures vary from 22°C to 28 °C in the rainy season and between 28 °C and 32 °C in the dry season. The precipitation regime is fairly regular. The peak rainfall regime appears in support of the idea that intense short duration rainfall is a main factor in landslides trigger in this region (Igwe et al. 2013).

Anambra State is derived from the Anambra Basin which is of the cretaceous age. The sedimentary formations in the basin, (Figure 3), include the Mamu, Ajali and Nsukka formations, respectively overlying each other conformably with the Nsukka formation being the youngest Cretaceous sequence. The Tertiary formations include the Palaeocene Imo Shale, overlain by the Eocene Ameki Formation/Nanka Sands, Ogwashi-Asaba Formation and Quaternary Alluvium, (Nwajide 1980; Whiteman, 1982; Nfor et al., 2007). The study area, Nnewi, falls under the Ogwashi-Asaba Formation (Oligocene-Miocene) which overlies the Ameki Formation (Eocene). The Ogwashi-Asaba Formation (Oligocene-Miocene) consists of fine to coarse grained pebbly unconsolidated sandstone with alternation of seam beds of lignite and clay

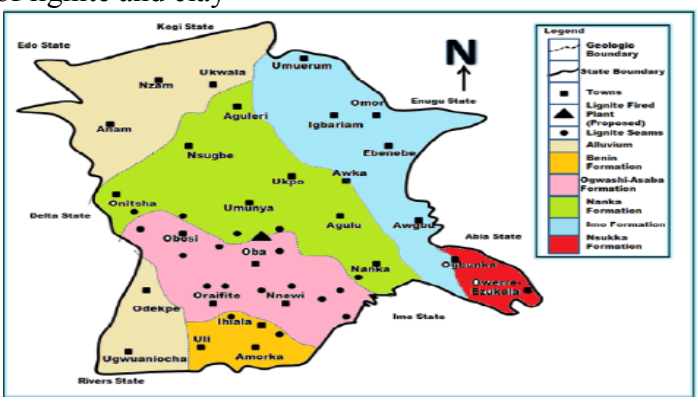

Figure 3. Geological Map of Anambra State showing Nnewi the Study Area (culled from Chikwelu et al., 2021).

2.0 Basic Theory

3.1 Geoelectrical Methods

The electrical resistivity method investigates subsurface conditions by injecting an electric current (I) using galvanic batteries (Direct Current) or low frequency alternating current (AC) generators into the ground through a pair of electrodes called current electrodes. The resulting potential difference (Δv) arising from the current flow is measured through a pair of another electrodes called potential electrodes which may or may not be located within the current electrode pair (Figure 4). The relationship between injected electric current, subsurface resistivity and resulting potential difference is provided by Ohm's Law.

$$\rho = \frac{\partial R \partial A}{\partial L} \quad 5$$

However, the subsurface is heterogeneous in nature, hence, apparent resistivity is the term used for the field measurements based on the geometric factors (G) of the electrode array used. The true image of the subsurface resistivity values is obtained through inversion of the apparent resistivity values at an acceptable range of Root Mean Square (RMS) values between observed and calculated resistivity values (Perrone et al., 2014; Rezaei et al., 2019).

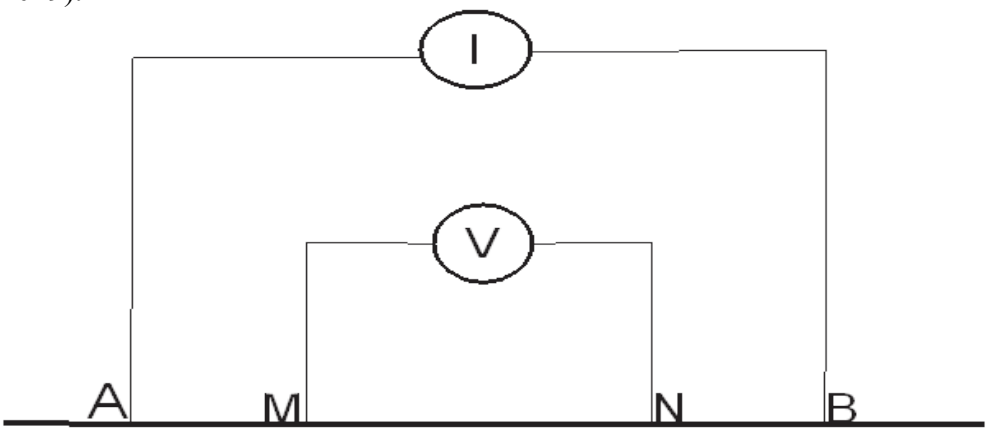

Figure 4. The generalized electrode configuration in resistivity method (kearey et al., 2002)

Geological materials have different electrical properties. The variations in these properties are useful geophysical parameters for characterizing geological materials. Subsurface variations in electrical resistivity typically correlate with variations in water content, fluid conductivity, porosity, permeability and the presence of metal. These variations may be used to locate subsurface features whose electrical properties contrast with the host material (Bisdorf and Lucius, 1999). The geoelectrical section has boundaries between layers determined by resistivity

contrast. To convert the resistivity picture into a geological picture, some knowledge of typical resistivity values for different types of subsurface materials and the geology of the area surveyed, is important (Table 1). A collection of published electrical resistivity values for different lithological units within Anambra State is presented in Table 2.

Table 1. Resistivities of some common geological materials (modified after Loke, 2001and Evrett 2013)

Geomaterial	Resistivity (Ohm-m)
Salt water	0.1 – 1.0
Clay	1 – 100
Silty clay	28 – 80
Clayey silt	50 – 120
Wet/moist sand	20 – 200
Shale	1 – 500
Porous limestone	100 - 1000
Gravel and sand	800 – 10000
Conglomerates and sandstone	100 – 10000
Lignite, coal	10 – 800
Groundwater (fresh)	10 - 120

Table 2. Published electrical resistivity values within Anambra State

Lithological material	Resistivity (Ωm)	Area/Community	Reference
Water–saturated/wet sandstone	363 - 9107	Ogidi	Onyekwelu et al., 202
Sandy – clay	14 – 101	Nanka	Chikwelu et al,, 2021
gravel deposit	8000 – 25000		
fine – medium sand plus alluvium	200 - 1000		

3.0 Materials and Methods

3.1 2D Electrical Resistivity Imaging (ERI) Measurement

The ERI measurements were carried out using PASI 16-GL Terrameter (Figure 4).

Figure 4. A PASI electrical resistivity meter

Nine profiles labeled UP1 to UP9 were executed within the site and a control profile labeled UCI, executed on a residential street, about 700 m away from the landslide, (Figure 5). The nine profiles were aligned in approximately E-W direction while the control profile was taken in the N–S direction. The control profile was to establish the uneroded in-situ lithological units of the location. All the profiles measured 200 m in length. The Wenner-Schlumberger configuration was deployed due to its moderate sensitivity and high median depth of investigation, with 'a' value equaled as 10 m and 'n' value ranged from 1 to 8.

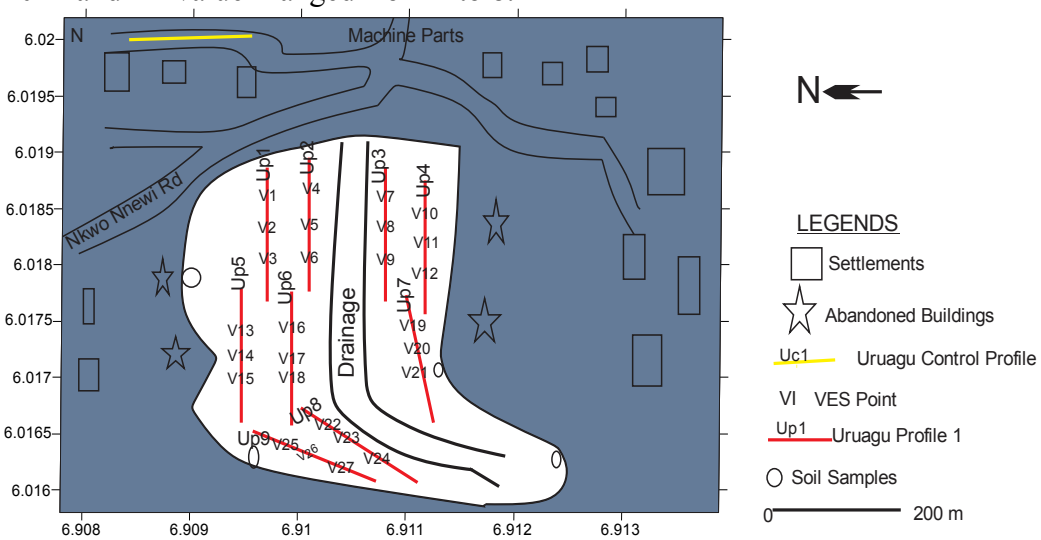

Figure 5. Site Study Map

The response of the ground was estimated as apparent resistivity (ρ_a) by multiplying the resistance recorded with the geometric factor (K) of the Wenner-Schlumberger array given in Equations 1 and 2.

$$\rho a = (\pi n(n+1)aR) \quad (1)$$

$$K = \pi n(n+1)a \quad (2)$$

The measured apparent resistivity field data were converted from text file format into readable format for inversion using the commercially available RES2DINV software package (Loke 2001). The software optimized a model of the resistivity distribution of the subsurface under investigation using 2-D finite element (FE) or finite difference (FD) techniques in order to allow the model potentials come as close as possible to the measured values. For inversion, both L_1 and L_2-norm options available

were tested (Loke et al., 2003). The L_1-norm model which produced smaller errors was presented in this study. Identical inversion parameters were used to process the resistivity measurements made along the profiles in order to minimize the model misfit. The best resistivity model was selected by successive calculations through iteration process of the model and the data. The model misfit describes how close the observed resistivity data was from the measured resistivity data

3.2 Vertical Electrical Sounding (VES) Measurement

In a quest to achieve a proper ground calibration, three VES were executed at points 80 m, 100 m and 120 m along each profile, making a total of 60 VES. The classical Schlumberger array was deployed with the same survey parameters in ERI. The maximum current electrode separation (AB) was 130m. The response of the ground was estimated as apparent resistivity (ρ_a) by multiplying the resistance (R) recorded with the geometric factor (K) of the Schlumberger array given in Equations 3 and 4.

$$\rho a = (0.5\pi(L\^2 - a\^2)R)/a \quad (3)$$

$$K = (0.5\pi(L\^2 - a\^2)R)/a \quad (4)$$

where L = half-length of current electrode separation

a = half-length of potential electrode separation

The VES apparent resistivity data were first plotted on log-log graph against half current electrodes separation (AB/2). The plotted data were then curved matched and true lithological unit resistivities and their corresponding depths/thicknesses calculated. The calculated parameters were then used as initial models in commercially available WinResist 1.0. The software iteratively correlated the field curve and the theoretical curve and determined the true resistivities and thicknesses of the mapped lithological units at very acceptable root mean square value (RMS <10%)

3.3 Soil Sample Laboratory Analysis

In other to have some ground truth knowledge of the site for the geoelectrical validation, following the counteraction work of the state government and erosion of some in-situ soils units, four disturbed soil samples were taken site at depths from their exposed in-situ limbs and outcrops, Physical and geotechnical laboratory index assessment (grain size, moisture content, Atterberg limits) were analyzed following standard procedures and methods for soil testing. Atterberg limit tests (liquid limit[LL], plastic limit[PL], and shrinkage limit[SL]) are standardized tests

that accurately define the strength, consistency and behavior boundaries between the solid, semi-solid, plastic, and liquid states of expansive (clay and silt) soils using moisture contents at the points where the physical changes occur, (Figure 6)

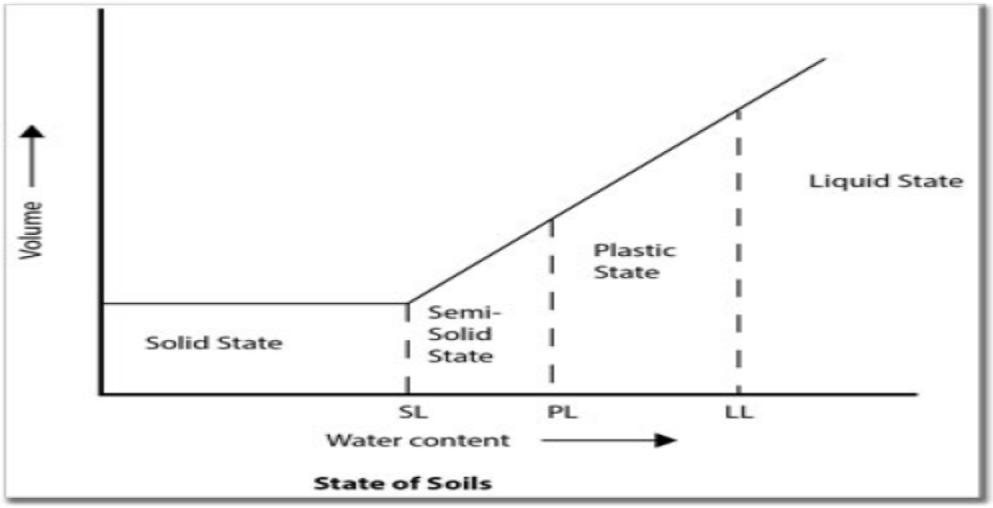

Figure 6. Atterberg limit consistency states of soils

The plasticity index (PI = PL – LL) indicates the size of the range between the two boundaries. Soils with a high PI have higher clay content. If the PI value is higher than the low to mid-20s, the soil may be expansive under wet conditions or exhibit shrinkage in dry conditions (Das,1998). Figure 7 and Table 3 present the plasticity chart and plasticity index classification respectively.

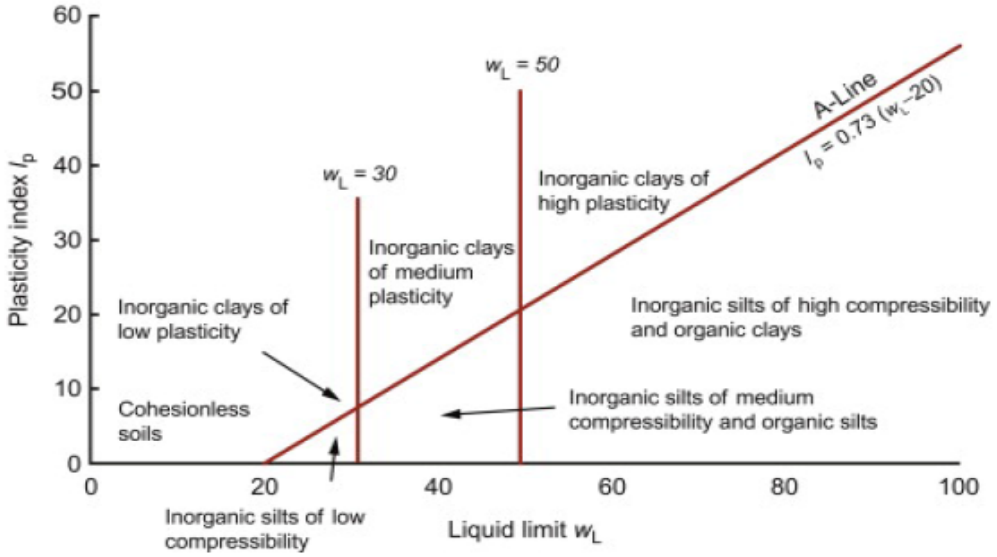

Figure 7. Plasticity Chart (after Casargande 1932)

Table 3. Plasticity Index classification (after Das,1998)

Plasticity Index (I_p)	Description
0	non plastic
1 - 5	Slightly plastic
5 - 10	Low plasticity
10 - 20	Medium plasticity
20- 40	High plasticity
>40	Very high plasticity

4.0 Results and Discussion

4.1 Results

4.1.1 Inverse ERI Models

The inverted 2D resistivity sections and their corresponding VES geoelectric sections along all the profiles are presented in Figure 8 (a – j).

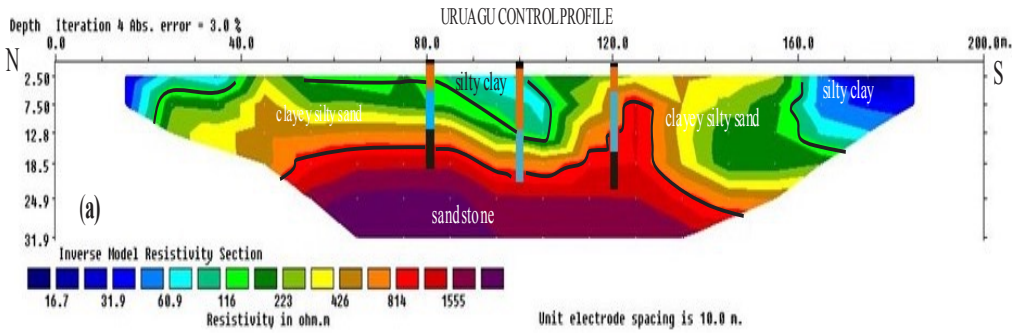

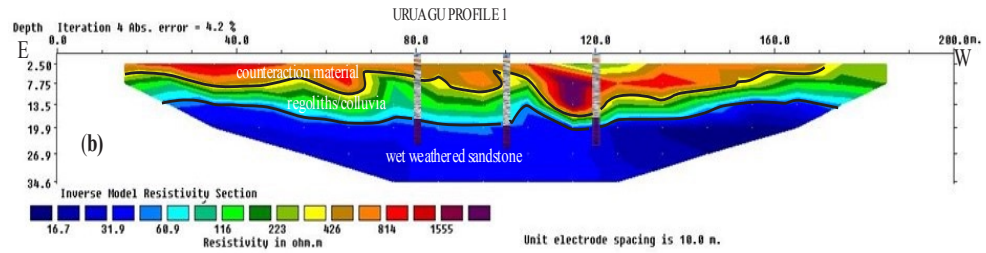

URUAGU PROFILE 2

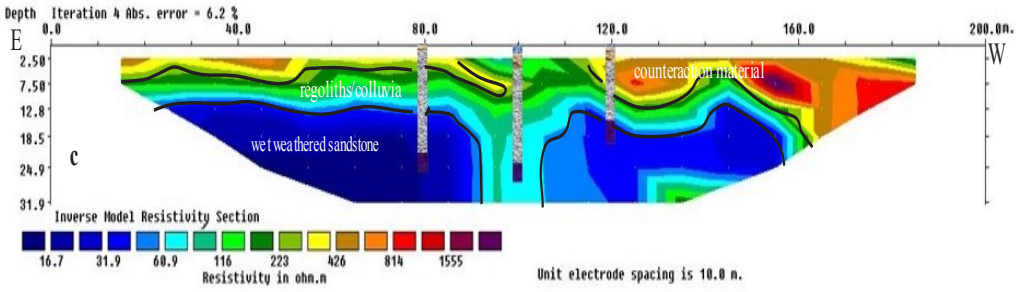

URUAGU PROFILE 3

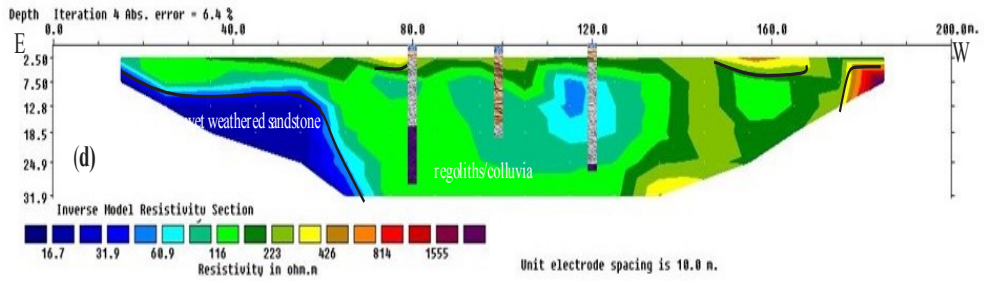

URUAGU PROFILE 4

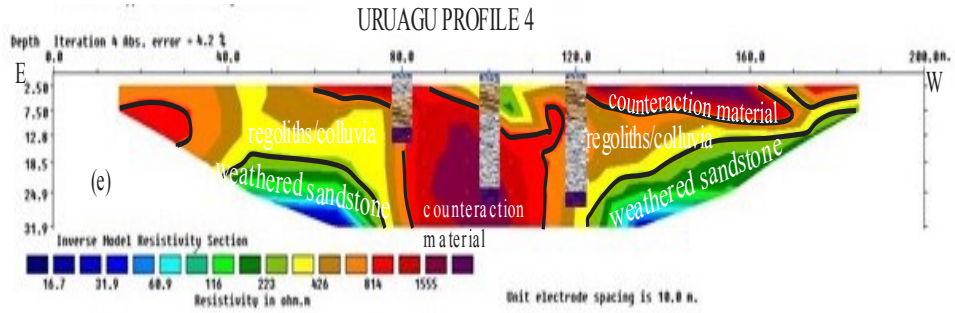

URUAGU PROFILE 5

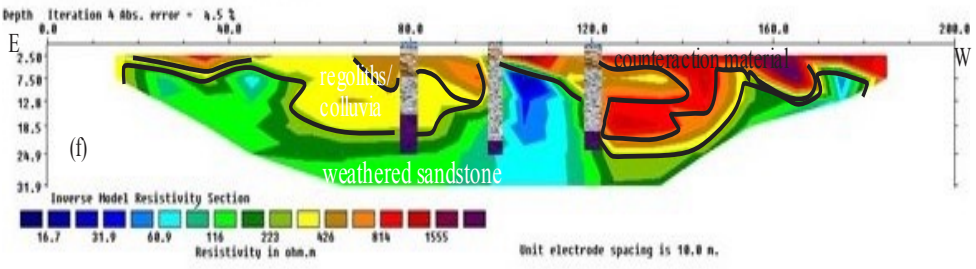

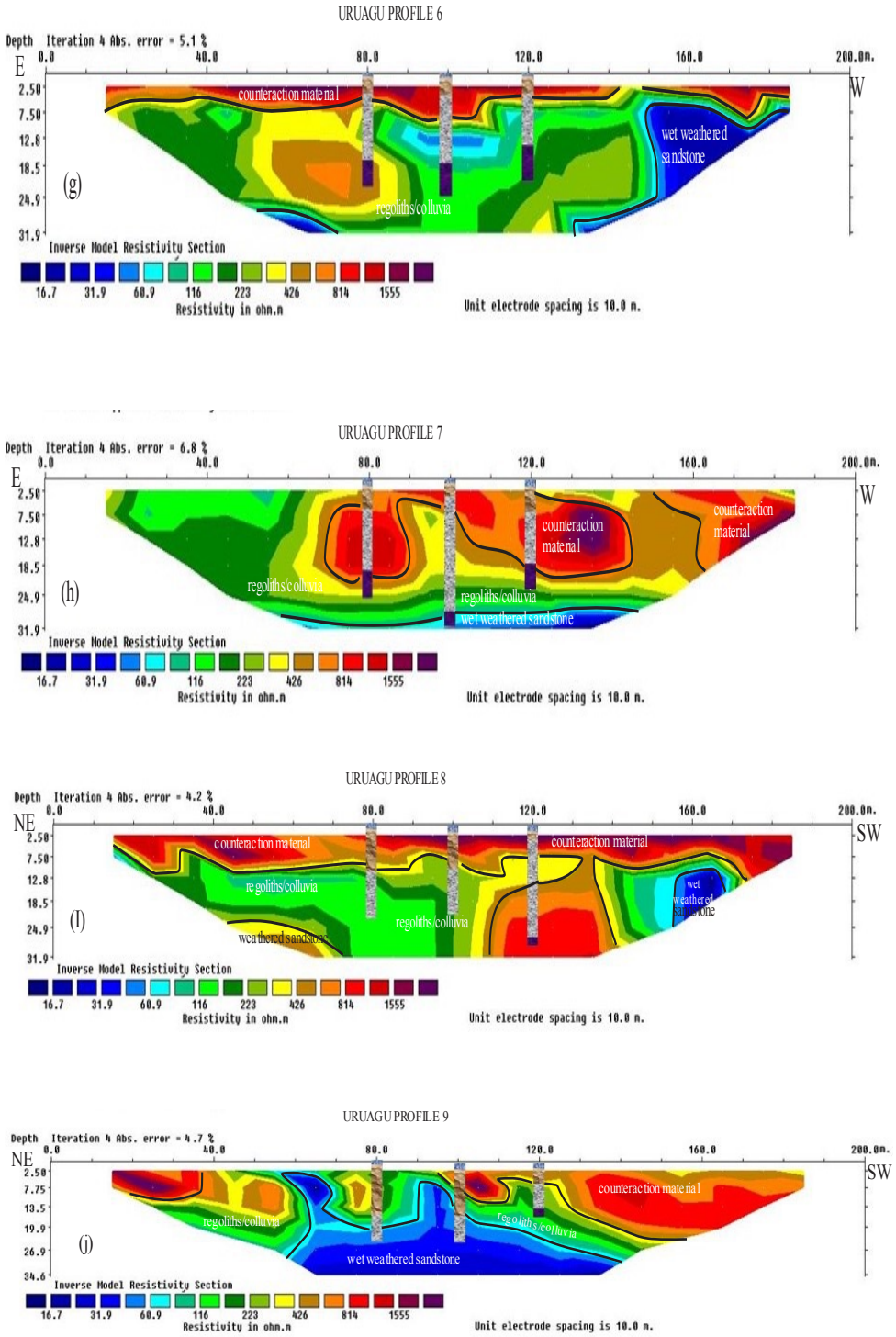

Figure 8. 2D Inverse Resistivity Models along the Profiles

4.1.2 Inverse VES Models

The inverted VES (1D) models which reflected the vertical variations of resistivity values as function of depth point for the investigated two landslide sites are presented in Figure 9 (CV1 to CV3, V1to V27).

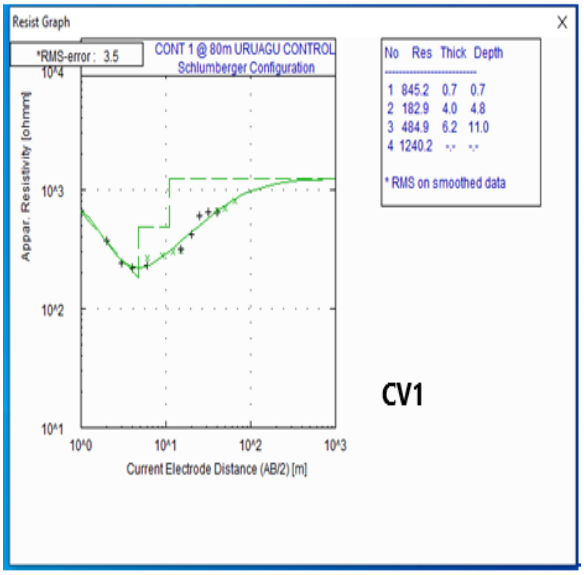

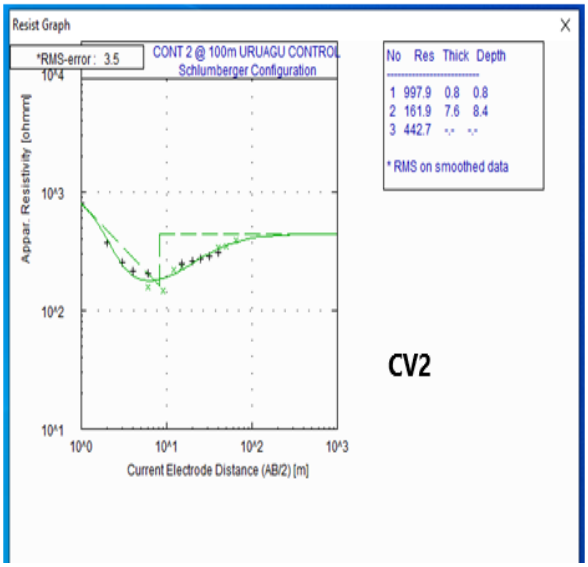

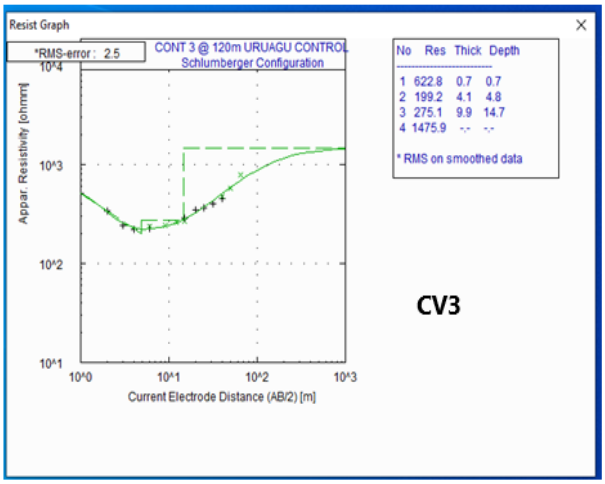
Resist Graph
*RMS-error : 2.5
CONT 3 @ 120m URUAGU CONTROL
Schlumberger Configuration
Appar. Resistivity [ohmm]
10^4
10^3
10^2
10^1
10^0
10^1
10^2
10^3
Current Electrode Distance (AB/2) [m]
No Res Thick Depth
1 622.8 0.7 0.7
2 199.2 4.1 4.8
3 275.1 9.9 14.7
4 1475.9 -.- -.-
* RMS on smoothed data
CV3

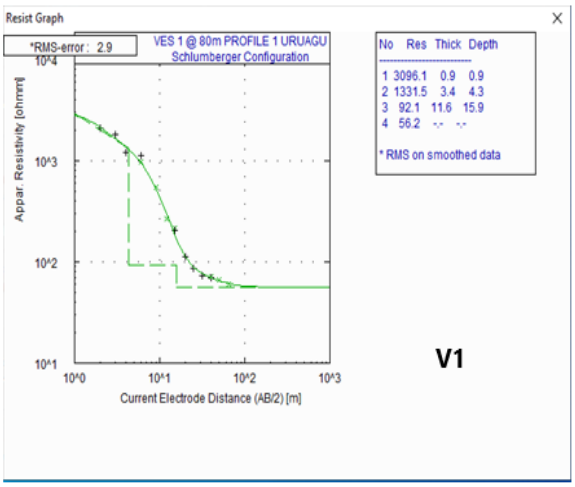
Resist Graph
*RMS-error : 2.9
VES 1 @ 80m PROFILE 1 URUAGU
Schlumberger Configuration
Appar. Resistivity [ohmm]
10^4
10^3
10^2
10^1
10^0
10^1
10^2
10^3
Current Electrode Distance (AB/2) [m]
No Res Thick Depth
1 3096.1 0.9 0.9
2 1331.5 3.4 4.3
3 92.1 11.6 15.9
4 56.2 -.- -.-
* RMS on smoothed data
V1

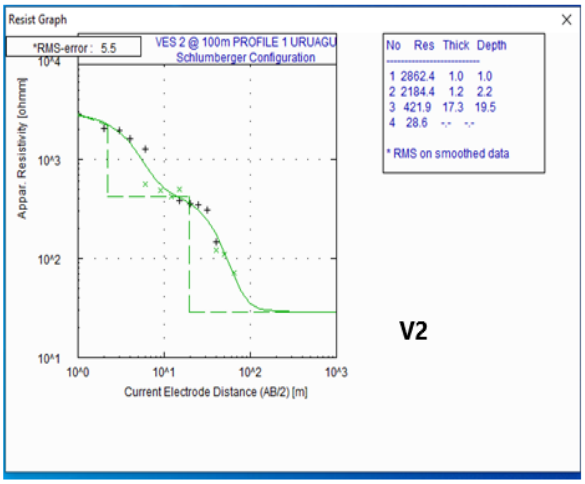
Resist Graph
*RMS-error : 5.5
VES 2 @ 100m PROFILE 1 URUAGU
Schlumberger Configuration
Appar. Resistivity [ohmm]
10^4
10^3
10^2
10^1
10^0
10^1
10^2
10^3
Current Electrode Distance (AB/2) [m]
No Res Thick Depth
1 2862.4 1.0 1.0
2 2184.4 1.2 2.2
3 421.9 17.3 19.5
4 28.6 -.- -.-
* RMS on smoothed data
V2

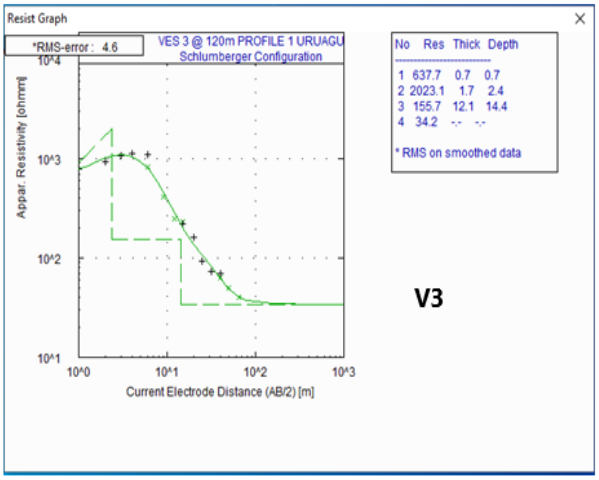
Resist Graph
*RMS-error : 4.6
VES 3 @ 120m PROFILE 1 URUAGU
Schlumberger Configuration
No Res Thick Depth
1 637.7 0.7 0.7
2 2023.1 1.7 2.4
3 155.7 12.1 14.4
4 34.2 -.- -.-
* RMS on smoothed data
Appar. Resistivity [ohmm]
10^4
10^3
10^2
10^1
10^0 10^1 10^2 10^3
Current Electrode Distance (AB/2) [m]
V3

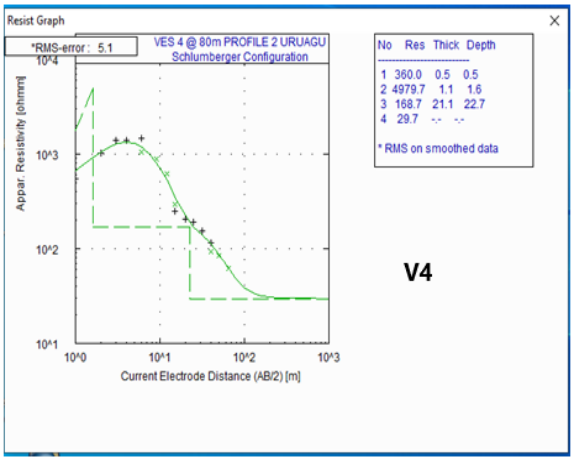
Resist Graph
*RMS-error : 5.1
VES 4 @ 80m PROFILE 2 URUAGU
Schlumberger Configuration
No Res Thick Depth
1 360.0 0.5 0.5
2 4979.7 1.1 1.6
3 168.7 21.1 22.7
4 29.7 -.- -.-
* RMS on smoothed data
Appar. Resistivity [ohmm]
10^4
10^3
10^2
10^1
10^0 10^1 10^2 10^3
Current Electrode Distance (AB/2) [m]
V4

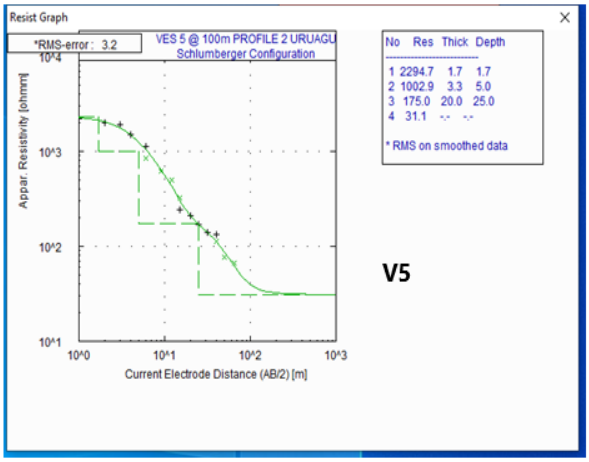
Resist Graph
*RMS-error : 3.2
VES 5 @ 100m PROFILE 2 URUAGU
Schlumberger Configuration
No Res Thick Depth
1 2294.7 1.7 1.7
2 1002.9 3.3 5.0
3 175.0 20.0 25.0
4 31.1 -.- -.-
* RMS on smoothed data
Appar. Resistivity [ohmm]
10^4
10^3
10^2
10^1
10^0 10^1 10^2 10^3
Current Electrode Distance (AB/2) [m]
V5

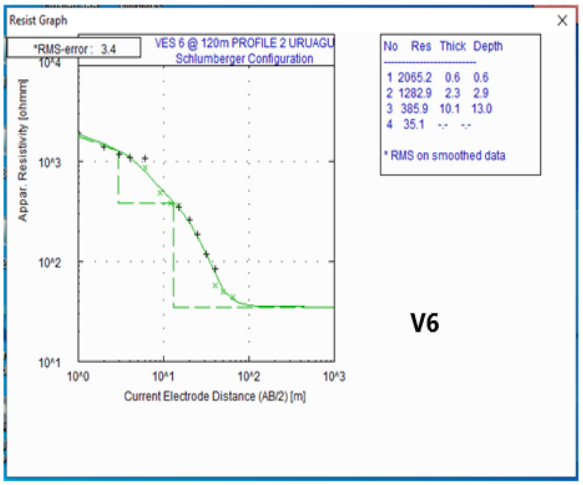
Resist Graph
*RMS-error : 3.4
VES 6 @ 120m PROFILE 2 URUAGU
Schlumberger Configuration
No Res Thick Depth
1 2065.2 0.6 0.6
2 1282.9 2.3 2.9
3 385.9 10.1 13.0
4 35.1 -.- -.-
* RMS on smoothed data
Appar. Resistivity [ohmm]
10^4
10^3
10^2
10^1
10^0 10^1 10^2 10^3
Current Electrode Distance (AB/2) [m]
V6

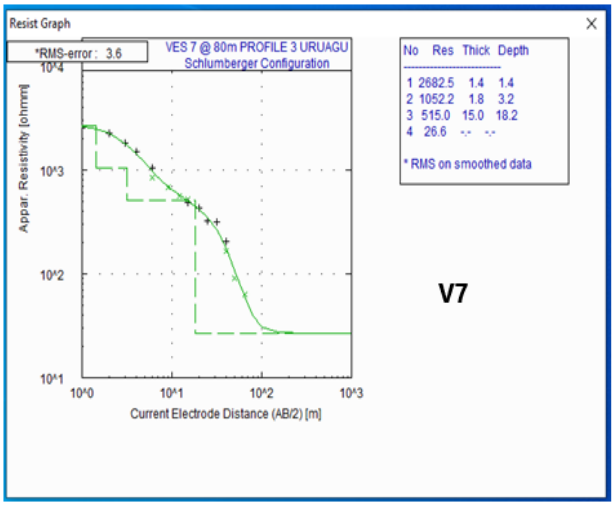
Resist Graph
*RMS-error : 3.6
VES 7 @ 80m PROFILE 3 URUAGU
Schlumberger Configuration
No Res Thick Depth
1 2682.5 1.4 1.4
2 1052.2 1.8 3.2
3 515.0 15.0 18.2
4 26.6 -.- -.-
* RMS on smoothed data
Appar. Resistivity [ohmm]
10^4
10^3
10^2
10^1
10^0 10^1 10^2 10^3
Current Electrode Distance (AB/2) [m]
V7

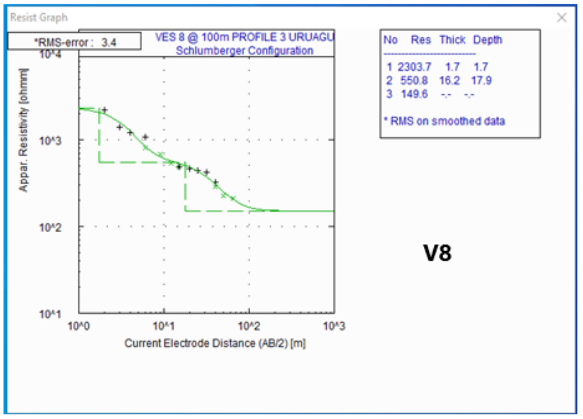
Resist Graph
*RMS-error : 3.4
VES 8 @ 100m PROFILE 3 URUAGU
Schlumberger Configuration
No Res Thick Depth
1 2303.7 1.7 1.7
2 550.8 16.2 17.9
3 149.6 -.- -.-
* RMS on smoothed data
Appar. Resistivity [ohmm]
10^4
10^3
10^2
10^1
10^0 10^1 10^2 10^3
Current Electrode Distance (AB/2) [m]
V8

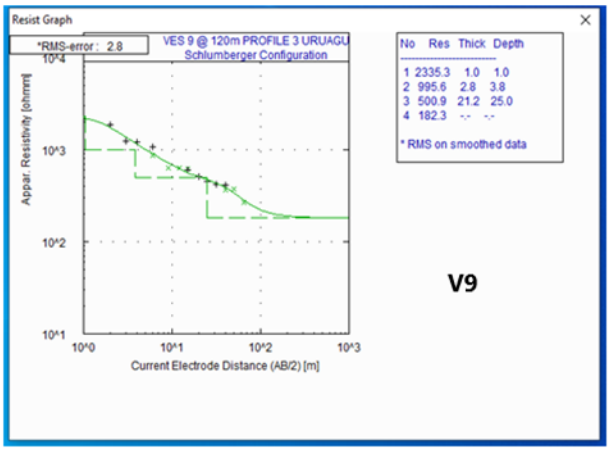
Resist Graph
*RMS-error : 2.8
VES 9 @ 120m PROFILE 3 URUAGU
Schlumberger Configuration
Appar. Resistivity [ohmm]
10^4
10^3
10^2
10^1
10^0
10^1
10^2
10^3
Current Electrode Distance (AB/2) [m]
No Res Thick Depth
1 2335.3 1.0 1.0
2 995.6 2.8 3.8
3 500.9 21.2 25.0
4 182.3 -.- -.-
* RMS on smoothed data
V9

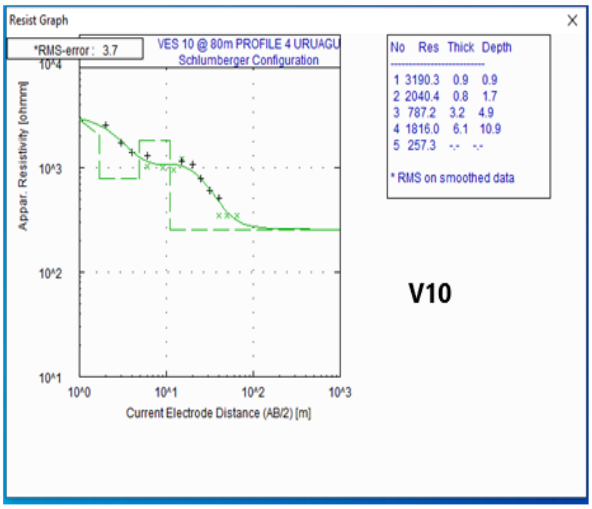
Resist Graph
*RMS-error : 3.7
VES 10 @ 80m PROFILE 4 URUAGU
Schlumberger Configuration
Appar. Resistivity [ohmm]
10^4
10^3
10^2
10^1
10^0
10^1
10^2
10^3
Current Electrode Distance (AB/2) [m]
No Res Thick Depth
1 3190.3 0.9 0.9
2 2040.4 0.8 1.7
3 787.2 3.2 4.9
4 1816.0 6.1 10.9
5 257.3 -.- -.-
* RMS on smoothed data
V10

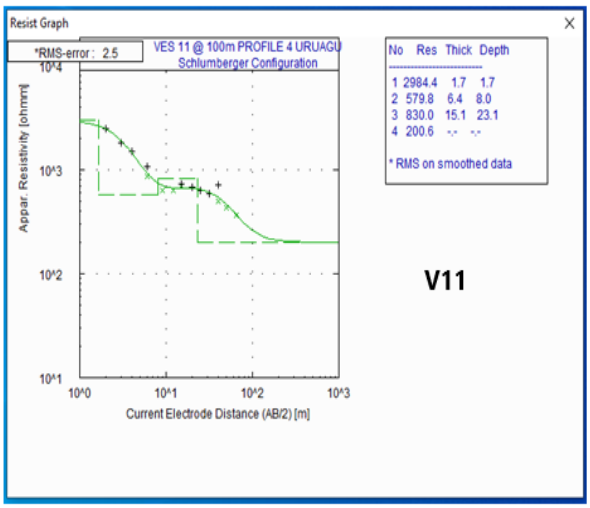
Resist Graph
*RMS-error : 2.5
VES 11 @ 100m PROFILE 4 URUAGU
Schlumberger Configuration
Appar. Resistivity [ohmm]
10^4
10^3
10^2
10^1
10^0
10^1
10^2
10^3
Current Electrode Distance (AB/2) [m]
No Res Thick Depth
1 2984.4 1.7 1.7
2 579.8 6.4 8.0
3 830.0 15.1 23.1
4 200.6 -.- -.-
* RMS on smoothed data
V11

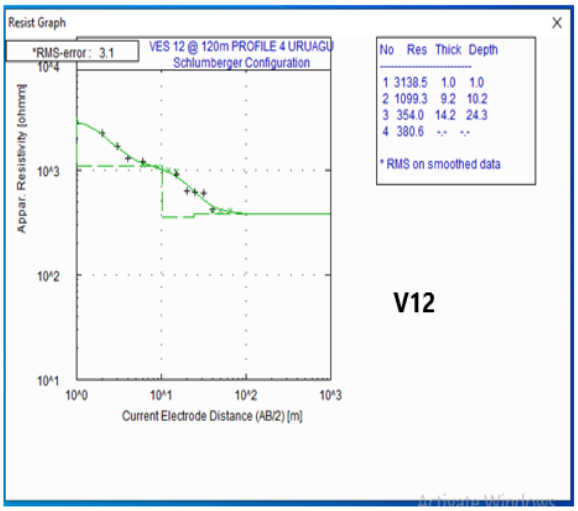
Resist Graph
*RMS-error : 3.1
VES 12 @ 120m PROFILE 4 URUAGU
Schlumberger Configuration
Appar. Resistivity [ohmm]
10^4
10^3
10^2
10^1
10^0
10^1
10^2
10^3
Current Electrode Distance (AB/2) [m]
No Res Thick Depth
1 3138.5 1.0 1.0
2 1099.3 9.2 10.2
3 354.0 14.2 24.3
4 380.6 -.- -.-
* RMS on smoothed data
V12

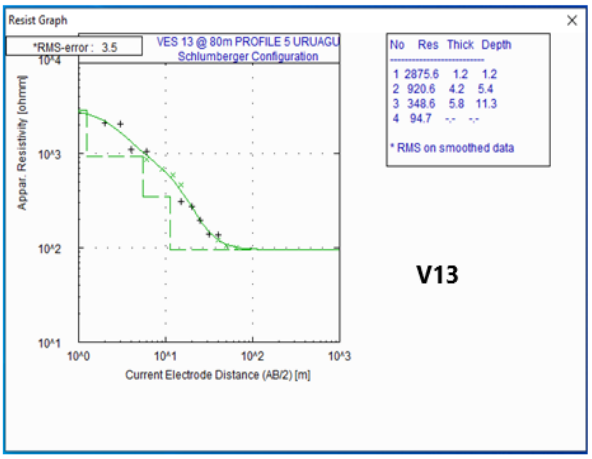
Resist Graph
*RMS-error : 3.5
VES 13 @ 80m PROFILE 5 URUAGU
Schlumberger Configuration
Appar. Resistivity [ohmm]
10^4
10^3
10^2
10^1
10^0
10^1
10^2
10^3
Current Electrode Distance (AB/2) [m]
No Res Thick Depth
1 2875.6 1.2 1.2
2 920.6 4.2 5.4
3 348.6 5.8 11.3
4 94.7 -.- -.-
* RMS on smoothed data
V13

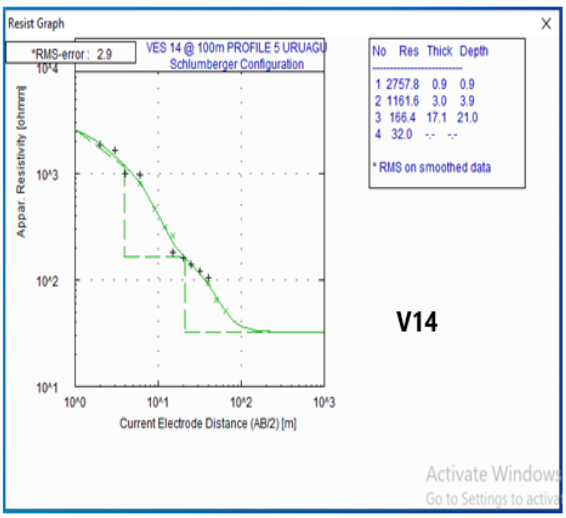
Resist Graph
*RMS-error : 2.9
VES 14 @ 100m PROFILE 5 URUAGU
Schlumberger Configuration
Appar. Resistivity [ohmm]
10^4
10^3
10^2
10^1
10^0
10^1
10^2
10^3
Current Electrode Distance (AB/2) [m]
No Res Thick Depth
1 2757.8 0.9 0.9
2 1161.6 3.0 3.9
3 166.4 17.1 21.0
4 32.0 -.- -.-
* RMS on smoothed data
V14
Activate Windows
Go to Settings to activa

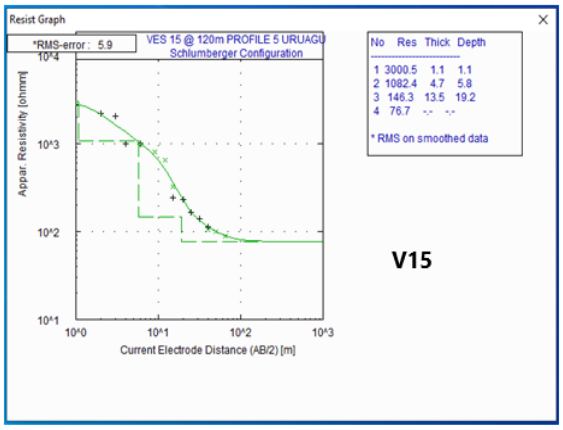
Resist Graph
*RMS-error : 5.9
VES 15 @ 120m PROFILE 5 URUAGU
Schlumberger Configuration
No Res Thick Depth
1 3000.5 1.1 1.1
2 1082.4 4.7 5.8
3 146.3 13.5 19.2
4 76.7 -.- -.-
* RMS on smoothed data
Appar. Resistivity [ohmm]
Current Electrode Distance (AB/2) [m]
V15

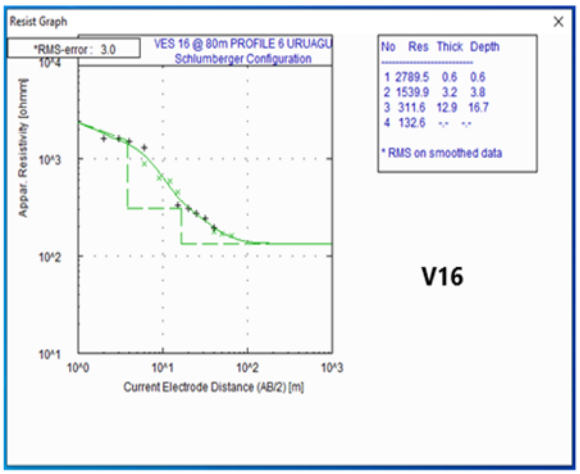
Resist Graph
*RMS-error : 3.0
VES 16 @ 80m PROFILE 6 URUAGU
Schlumberger Configuration
No Res Thick Depth
1 2789.5 0.6 0.6
2 1539.9 3.2 3.8
3 311.6 12.9 16.7
4 132.6 -.- -.-
* RMS on smoothed data
Appar. Resistivity [ohmm]
Current Electrode Distance (AB/2) [m]
V16

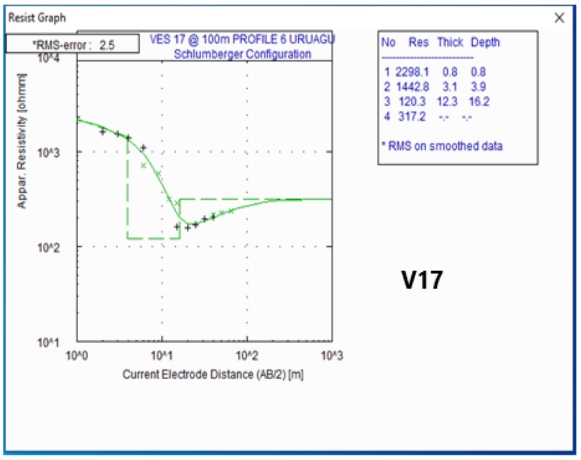
Resist Graph
*RMS-error : 2.5
VES 17 @ 100m PROFILE 6 URUAGU
Schlumberger Configuration
No Res Thick Depth
1 2298.1 0.8 0.8
2 1442.8 3.1 3.9
3 120.3 12.3 16.2
4 317.2 -.- -.-
* RMS on smoothed data
Appar. Resistivity [ohmm]
Current Electrode Distance (AB/2) [m]
V17

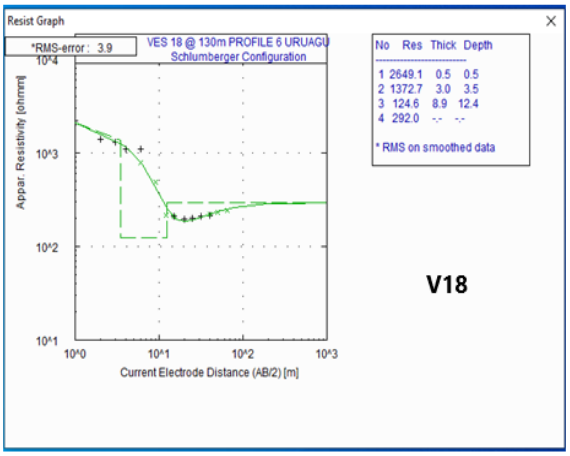
Resist Graph
*RMS-error : 3.9
VES 18 @ 130m PROFILE 6 URUAGU
Schlumberger Configuration
No Res Thick Depth
1 2649.1 0.5 0.5
2 1372.7 3.0 3.5
3 124.6 8.9 12.4
4 292.0 -.- -.-
* RMS on smoothed data
Appar. Resistivity [ohmm]
10^4
10^3
10^2
10^1
10^0 10^1 10^2 10^3
Current Electrode Distance (AB/2) [m]
V18

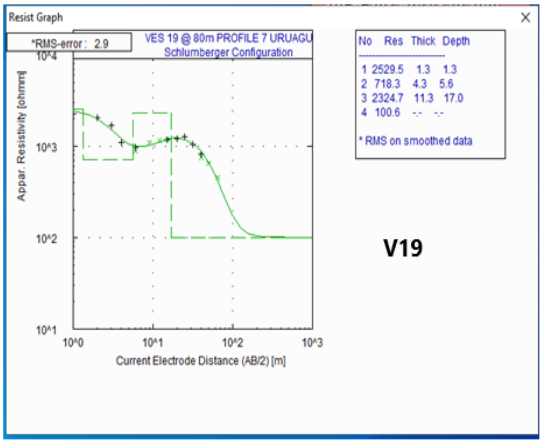
Resist Graph
*RMS-error : 2.9
VES 19 @ 80m PROFILE 7 URUAGU
Schlumberger Configuration
No Res Thick Depth
1 2529.5 1.3 1.3
2 718.3 4.3 5.6
3 2324.7 11.3 17.0
4 100.6 -.- -.-
* RMS on smoothed data
Appar. Resistivity [ohmm]
10^4
10^3
10^2
10^1
10^0 10^1 10^2 10^3
Current Electrode Distance (AB/2) [m]
V19

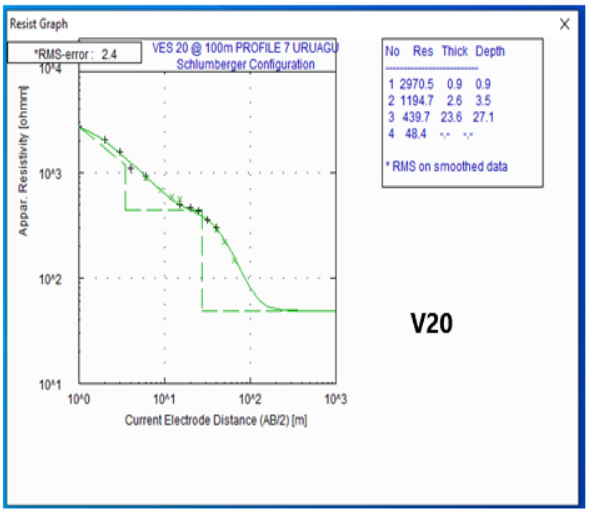
Resist Graph
*RMS-error : 2.4
VES 20 @ 100m PROFILE 7 URUAGU
Schlumberger Configuration
No Res Thick Depth
1 2970.5 0.9 0.9
2 1194.7 2.6 3.5
3 439.7 23.6 27.1
4 48.4 -.- -.-
* RMS on smoothed data
Appar. Resistivity [ohmm]
10^4
10^3
10^2
10^1
10^0 10^1 10^2 10^3
Current Electrode Distance (AB/2) [m]
V20

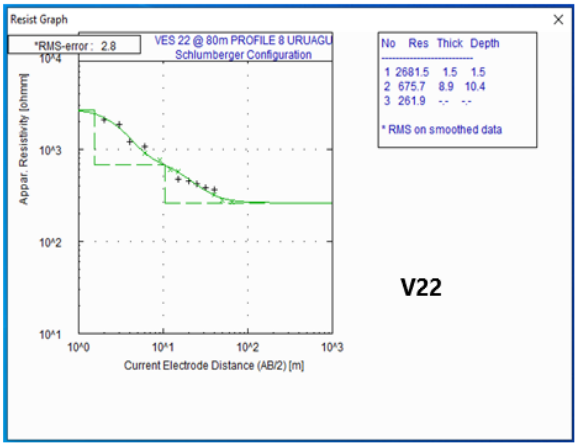
Resist Graph
*RMS-error : 2.8
VES 22 @ 80m PROFILE 8 URUAGU
Schlumberger Configuration
Appar. Resistivity [ohmm]
10^4
10^3
10^2
10^1
10^0
10^1
10^2
10^3
Current Electrode Distance (AB/2) [m]
No Res Thick Depth
1 2681.5 1.5 1.5
2 675.7 8.9 10.4
3 261.9 -.- -.-
* RMS on smoothed data
V22

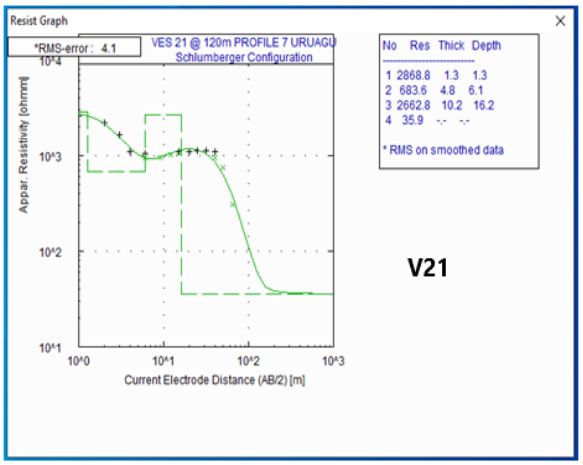
Resist Graph
*RMS-error : 4.1
VES 21 @ 120m PROFILE 7 URUAGU
Schlumberger Configuration
Appar. Resistivity [ohmm]
10^4
10^3
10^2
10^1
10^0
10^1
10^2
10^3
Current Electrode Distance (AB/2) [m]
No Res Thick Depth
1 2868.8 1.3 1.3
2 683.6 4.8 6.1
3 2662.8 10.2 16.2
4 35.9 -.- -.-
* RMS on smoothed data
V21

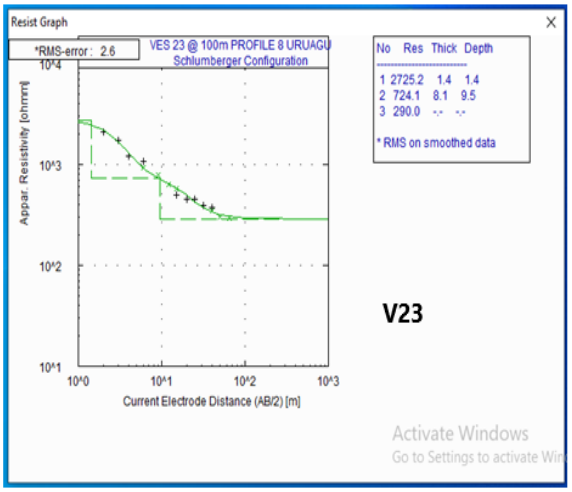
Resist Graph
*RMS-error : 2.6
VES 23 @ 100m PROFILE 8 URUAGU
Schlumberger Configuration
Appar. Resistivity [ohmm]
10^4
10^3
10^2
10^1
10^0
10^1
10^2
10^3
Current Electrode Distance (AB/2) [m]
No Res Thick Depth
1 2725.2 1.4 1.4
2 724.1 8.1 9.5
3 290.0 -.- -.-
* RMS on smoothed data
V23
Activate Windows
Go to Settings to activate Win

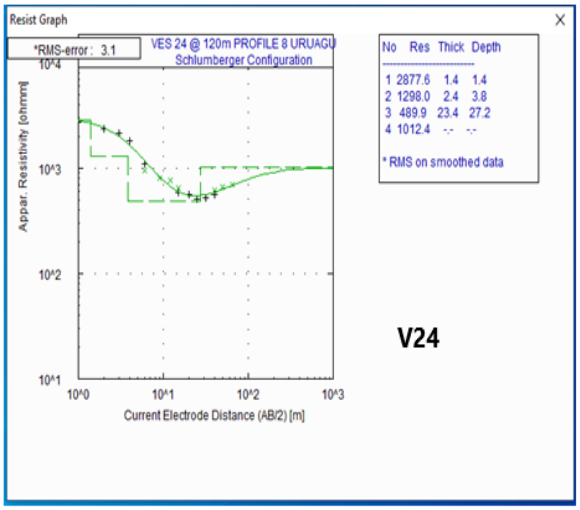
Resist Graph
*RMS-error : 3.1
VES 24 @ 120m PROFILE 8 URUAGU
Schlumberger Configuration
No Res Thick Depth
1 2877.6 1.4 1.4
2 1298.0 2.4 3.8
3 489.9 23.4 27.2
4 1012.4 -.- -.-
* RMS on smoothed data
Appar. Resistivity [ohmm]
10^4
10^3
10^2
10^1
10^0
10^1
10^2
10^3
Current Electrode Distance (AB/2) [m]
V24

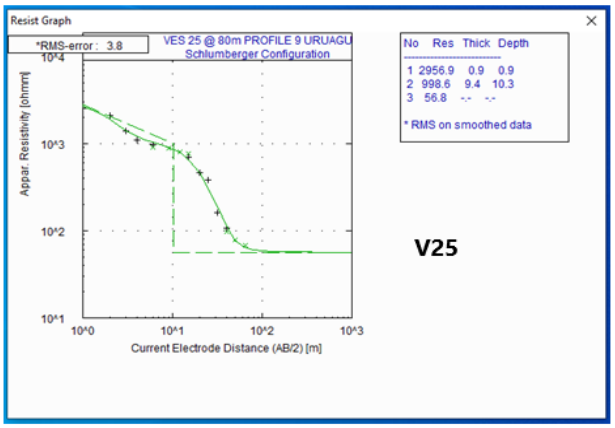
Resist Graph
*RMS-error : 3.8
VES 25 @ 80m PROFILE 9 URUAGU
Schlumberger Configuration
No Res Thick Depth
1 2956.9 0.9 0.9
2 998.6 9.4 10.3
3 56.8 -.- -.-
* RMS on smoothed data
Appar. Resistivity [ohmm]
10^4
10^3
10^2
10^1
10^0
10^1
10^2
10^3
Current Electrode Distance (AB/2) [m]
V25

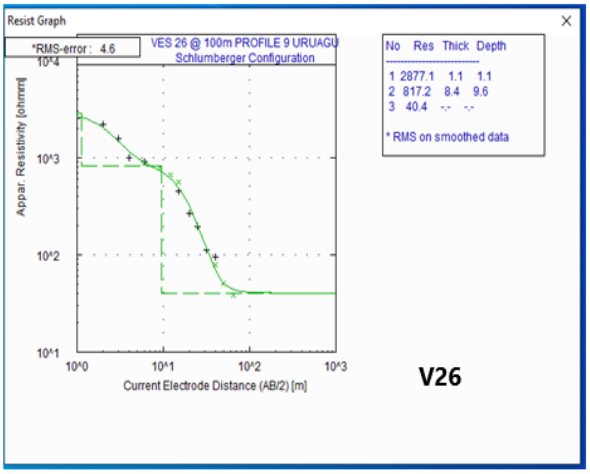
Resist Graph
*RMS-error : 4.6
VES 26 @ 100m PROFILE 9 URUAGU
Schlumberger Configuration
No Res Thick Depth
1 2877.1 1.1 1.1
2 817.2 8.4 9.6
3 40.4 -.- -.-
* RMS on smoothed data
Appar. Resistivity [ohmm]
10^4
10^3
10^2
10^1
10^0
10^1
10^2
10^3
Current Electrode Distance (AB/2) [m]
V26

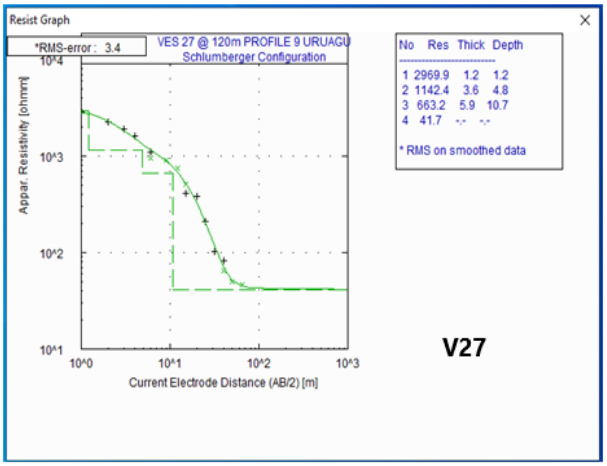

Figure 9. 1D Inverse Resistivity Models along the Profiles

4.1.3 Laboratory Results

The results of the four disturbed soil samples taken from site are presented as soil texture description (Table 4), particle size distribution by wet-sieving (Table 5) and Atterberg limit tests (Table 6)

Table 4. Soil texture description

Sample Nos.	Description of Soil
Uruagu(1)	silty sandy Clay
Uruagu(2)	Brown silty clay
Uruagu (3)	Brown, sandy silty clay.
Uruagu (4)	Reddish brown sandstone

Table 5. Particle Size Distribution by wet- sieving

Sample Nos.	Natural water content (wc%)	PERCENTAGE PARTICLE PASSING BY DRY WT				
		2.0 mm	0.600 mm	0.425 mm	0.300 mm	0.075mm
Uruagu (1)	11.0	97.0	85.0	80.0	77.0	70.0
Uruagu (2)	10.8	98.0	84.0	81.0	76.0	68.0
Uruagu (3)	10.6	97.0	85.0	80.0	77.0	70.0
Uruagu (4)	14.0	99.0	90.0	86.0	83.0	80.0

Table 6. Atterberg limit tests

Sample Nos.	Natural Water content (wc%)	Liquid Limit (L.L%)	Plastic Limit (P.L%)	Plasticity Index (P.I%)
Uruagu (1)	11.0	44.0	16.0	28.0
Uruagu (2)	10.8	46.0	17.0	29.0
Uruagu (3)	10.6	45.0	16.0	29.0
Uruagu (4)	14.0	-	-	-

4.2 Discussions

4.2.1 Inverse ERI Models

The control site profile (Figure 8a), executed on a residential street of even topography about 700 m from the landslide site, establishes knowledge of the in-situ local geological units of the site in line with existing geological information (Egbueri and Igwe, 2018; Onyekwelu et al., 2021). Three well layered geological units were mapped – silty clay, clayey silty sand and sandstone. The topsoil layer (silty clay) stretched throughout the model and is characterized with low resistivity range between 16.7 – 60.9 Ωm at depths 0 to about 13 m. Underlying the silty clay topsoil is the clayey silty sand unit. The resistivity value ranges from 116 - 800 Ωm at depth range of 2.5 m at a horizontal distance of 115 - 160 m down to 18.5 m. The sandstone is the third lithological unit with resistivity from 814 Ωm and above and depth variation of 7.5 m in the half space to 18.5 m at the ends of the profile. The section reveals well layered structures with the overlying two geological units relatively impermeable resulting in high resistivity values of the sandstone unit.

Profile 1 (Figure 8b), executed on the concave terrain of the landslide, at lower elevation and close to the adjoining road, revealed three geologic structures. Though, the in-situ lithologies have been eroded to various depths, the grain size laboratory analysis of the disturbed soils from the hanging flanks and outcrops establishes knowledge of the pre-existing local geological units in collaboration with the control profile. The first structure is the counteraction material with high resistivity value ranging from 814 Ωm and above, at depths 0 – 10 m. The counteraction material comprises majorly conglomerates of granite and laterites as observed on the site. They stretched throughout the profile length. The second geologic structure is predominantly the unconsolidated regoliths and colluvia of the landslide. This layer resistivity ranges from 116 - 300 Ωm and at varying depths of 7 to 13 m. The regoliths and colluvia include the intercalations of

slumped insitu silty clay, silty sandy clay, sandy silty clay and clayey silty sand units of the site as derived from the laboratory textural. The structure has undergone some diagenesis leading to it being more permeable, weak, easily dispersible and collapsible, following the uneven badland topography, high gully slope gradients, concave slopes (Figure 2) supported by Egbueri and Igwe (2018). The third geologic structure is the wet weathered sandstone unit. This layer is characterized by low resistivity values ranging from 16.7 – 60.9 Ωm and at depths variation of 13 m. The low resistivity values results from wetting of the soil matrix due to strong mechanical stresses during the landslide occurrence leading to water infiltration from the overlying regoliths and colluvia. The sandstone surface is the gliding/sliding surface the overlying layers slump or creep during failure.

Profile 2 (Figure 8c) also executed on the concave terrain of the landslide, also at lower elevation, revealed three geologic structures. The first structure is the counteraction material with high resistivity value ranging from 814 Ωm and above, at depths 0 – 13 m. This material is thinner along the horizontal distance till 120 m, indicative of the undulating surface before the counteraction work. The regoliths and colluvia unit underlies the counteraction material layer. The resistivity values range from 116 - 300 Ωm at vibrational depths of 2.5 m to 15 m. at a horizontal distance of 90 to 110 m appears a wider infiltration path to deeper depths. The sandstone unit, characterized by low resistivity values ranging from 16.7 – 60.9 Ωm and at depths variation of 13 m underlies the regoliths and colluvia unit. The low resistivity values results from wetting of the soil matrix due to strong mechanical stresses during the landslide occurrence leading to water infiltration from the overlying regoliths and colluvia.

Profiles 3 to 9, (Figures 8d- j), executed at different elevations within the convave terrain revealed the three geologic structures respectively. The different elevations of the profiles imparted the variations in depth and thicknesses of the structures.

4.2.2 Inverse VES Models

The VES for the Control Site Profile (Figure 9 CV1 – CV3) at points 80 m, 100 m and 120 m respectively, establishes point knowledge of the in-situ local geological units in validation of the ERI and as an alternative to geotechnical drilling. The CV1 sounding revealed four geoelectric units. The topsoil is dry sand of resistivity 845.2 Ωm and 0.7 m thickness. The silty clay with resistivity 182.9 Ωm and thickness 4.0 m underlies the topsoil. The clayey silty sand with resistivity 484.9 Ωm and thickness 6.2 m is the third layer. The sandstone layer underlies as the fourth unit with resistivity 1240.2 Ωm. The CV2 sounding mapped the first three units. The dry sand topsoil is of resistivity 997.9 Ωm and 0.9 m thickness. The silty clay unit has

resistivity of 161.9 Ωm and thickness 7.6 m. The clayey silty sand unit is mapped with resistivity 442.7 Ωm. The CV3 sounding revealed four geoelectric units. The topsoil is dry sand of resistivity 622.8 Ωm and 0.7 m thickness. The silty clay with resistivity 199.2 Ωm and thickness 4.1 m underlies the topsoil. The clayey silty sand with resistivity 275.1 Ωm and thickness 9.9 m is the third layer. The sandstone layer underlies as the fourth unit with resistivity 1475.9 Ωm. The dry sand topsoil is not mapped in the ERI section due to its larger minimum electrode spacing of 10m. This is the case with all profiles and their corresponding VES points. The VES for the concave terrain landslide site Profile 1 (Figure 9 V1 – V3) revealed four geologic structures. For the V1, the topsoil is loose counteraction material of resistivity 3095.1 Ωm and thickness 0.9 m. The second unit is the counteraction material layer of resistivity 1331.5 Ωm and thickness 3.4 m. The regoliths and colluvia with resistivity 92.1 Ωm and thickness 11.6 m underlies the counteraction material layer. The wet weathered sandstone is the fourth unit with resitivity 56.2 Ωm. The V2 sounding mapped the loose counteraction material topsoil with resistivity 2862.4 Ωm and thickness 1.0 m. The counteraction material second layer has resistivity 2184.4 Ωm and thickness 1.2 m. The regoliths and colluvia unit is mapped with resistivity 421.9 Ωm and thickness 27.3 m. The underlying wet weathered sandstone has resitivity value 28.6 Ωm. The V3 sounding revealed the loose counteraction material with resistivity value 637.7 Ωm and thickness 0.7 m. The counteraction material second layer is mapped with resistivity 2023.1 Ωm and thickness 1.7 m. The regoliths and colluvia unit is mapped with resistivity 155.7 Ωm and thickness 12.1 m. The underlying wet weathered sandstone is mapped with resistivity 34.2 Ωm. The VES for Profile 2 (Figure 9 V4 – V6) also revealed four geoelectric structures. For the V4, the topsoil is loose counteraction material of resistivity 360.0 Ωm and thickness 0.5 m. The second unit is the counteraction material layer of resistivity 4979.7 Ωm and thickness 1.1 m. The regoliths and colluvia with resistivity 168.7 Ωm and thickness 21.1 m underlies the counteraction material layer. The wet weathered sandstone is the fourth unit with resitivity 29.7 Ωm. The V5 sounding mapped the loose counteraction material topsoil with resistivity 2294.7 Ωm and thickness 1.7 m. The counteraction material second layer has resistivity 1002.9 Ωm and and thickness 3.3 m. The regoliths and colluvia are mapped with resistivity 175.0 Ωm and thickness 20.0 m. The wet weathered sandstone is the fourth unit with resitivity 31.1 Ωm. For the V6, the topsoil loose counteraction material has resistivity 2065.2 Ωm and thickness 0.6 m. The second unit is the counteraction material layer of resistivity 1282.9 Ωm and thickness 2.3m. The regoliths and colluvia with resistivity 385.9 Ωm and thickness 10.1 m underlies the counteraction material layer. The wet weathered sandstone is the fourth unit with resistivity

35.1 Ωm. The VES of the remaining profiles (Figure 9 V7 – V27) also revealed mostly four geoelectric structures as loose counteraction material topsoil, counteraction material second layer, regoliths and colluvia third layer, underlain by variably wet weathered sandstone.

4.2.3 Laboratory Results

The textural description (Table 4) derived from the particle size (Table 5) of the disturbed four samples revealed silty sandy clay, brown silty clay, brown sandy silty clay and reddish brown sandstones as the pre-landslide existing lithologies in no stratification order. Table 6 presents the Atterberg;s limits of the cohesive soils only. The silty sandy clay has 44% liquid limit (LL), 16% plastic limit (PL) and 28% plast icity index (PI). The brown silty clay has 46% liquid limit (LL), 17% plastic limit (PL) and 29% plasticity index (PI). The brown sandy silty clay has 45% liquid limit (LL), 15% plastic limit (PL) and 29% plasticity index (PI). These cohesive soils, (silty sandy clay, silty clay and sandy silty clay) from the plasticity chart (Figure 7), are above the A-Line and belong to the inorganic clays of medium plasticity. From the plasticity index classification (Table 3) only, the cohesive soils are classified as highly plastic. These soils during intense rainfall, imbibe more water, following their high plasticity, slided along the sandstone to activate the landside.

4.2.4 Comparison of ERI and VES Results

The correlation of inverse ERI models and their corresponding VES geoelectric sections along all the profiles is presented in Figure 8(a-j) and the inferred structures with depth, (Table 7). The ERI models revealed mostly three structures along the profiles The VES revealed majorly three to four structures.

Table 7. ERI and VES correlation

Profile	Layer	ERI		VES @80m		VES @100m		VES @ 120m		structure
		Resistivi.(Ωm)	Depth (m)	Ωm	Depth	Ωm	Depth	Ωm	Depth	
Control	0			845.2	0-0.7	997.9	0-0.8	622.8	0-0.7	Dry sand
	1	16.7-70.0	0-10	182.9	0.7-4.8	161.9	0.8-8.4	199.2	0.7-4.8	Silty clay
	2	116-430	10-20	484.9	4.8-21	442.7	8.4 □	275.1	4.8-14.7	Clayey silty sand
	3	>814	20-32	1240.2	11 □			1475.9	14.7□	sandstone

1	0			3096.1	0-0.9	2862.4	0-1.0	637.7	0-0.7	Loose counteraction
	1	>814	0-14	1331.5	0.9-4.3	2184.4	1.0-2.2	2023.1	0.7-2.4	Counteraction material
	2	116-430	14-20	92.1	4.3-15.9	421.9	2.2-19.5	155.7	2.4-14.5	Regoliths/colluvia
	3	16.7-70.0	20-35	56.2	15.9□	28.6	19.5□	34.2	14.5□	Wet weathered sandst.
2	0			360.0	0-0.5	2294.7	0-1.7	2055.2	0-0.5	Loose counteraction
	1	>814	0-13	4979.7	0.5-1.6	1002.9	1.7-5.0	1282.9	0.5-2.9	Counteraction material
	2	116-430	13-24	168.7	1.6-22.7	175.0	5.0-25.0	385.9	2.9-13.0	Regoliths/colluvia
	3	16.7-70.0	18-32	29.7	22.7□	31.1	25.0□	35.1	13.0□	Wet weathered sandst.
3	0			2682.5	0-1.4	2303.7	0-1.7	2335.3	0-1.0	Loose counteraction
	1	>814	0-2.5	1052.2	1.4-3.2	550.8	1.7-17.9	995.6	1.0-3.8	Counteraction material
	2	116-430	2.5-25	515.0	3.2-18.2	149.6	17.9□	500.9	3.8-25.0	Regoliths/colluvia
	3	16.7-70.0	7.5-32	26.6	18.2□			182.3	25.0□	Wet weathered sandst.
4	0			3190.3 2040.4	0-0.9 0.9-1.7	2984.4	0-1.7	3138.5	0-1.0	Loose counteraction
	1	>814	0-32	787.2	1.7-4.9	579.8	1.7-8.0	1099.3	1.0-10.2	Counteraction material
	2	116-430	2.5-32	1816.0	4.9-10.9	830.0	8.0-23.1	354.0	10.2-24.3	Regoliths/colluvia
	3	16.7-70.0	13-32	257.3	10.9□	200.5	23.1□	380.6	24.3□	Wet weathered sandst.

5	0			2875.6	0-1.2	2757.8	0-0.9	3000.5	0-1.1	Loose countera ction
	1	>814	0-13	920.6	1.2-5.4	1161.6	0.9-3.9	1082.4	1.1-5.8	Countera ction material
	2	116-430	2.5-19	348.6	5.4-11.3	166.4	3.9-21.0	146.3	5.8-19.2	Regolith s/colluvi a
	3	16.7-70.0	13-32	94.7	11.3□	32.0	21.0□	76.7	19.2□	weathere d sandst.
6	0			2789.5	0-0.6	2298.1	0-0.8	2649.1	0-0.5	Loose countera ction
	1	>814	0-8.0	1539.9	0.6-3.8	1442.8	0.8-3.9	1372.7	0.5-3.5	Countera ction material
	2	116-430	8.0-32	311.6	3.8-16.7	120.3	3.9-16.2	124.6	3.5-12.4	Regolith s/colluvi a
	3	16.7-70.0	13-32	132.6	16.7□	317.2	16.2□	292.0	12.4□	Wet weathere d sandst.
7	0			2529.5	0-1.3	2970.5	0-0.9	2868.8	0-1.3	Loose countera ction
	1	>814	0-19	718.3	1.3-5.6	1194.7	0.9-3.5	683.6	1.3-6.1	Countera ction material
	2	116-430	2.5-30	2324.7	6.6-17	439.7	3.5-27.1	2662.8	6.1-16.2	Regolith s/colluvi a
	3	16.7-70.0	30-32	100.6	17.0□	48.4	27.1□	35.9	16.2□	Wet weathere d sandst.
8	0			2681.5	0-1.5	2725.2	0-1.4	2877.6	0-1.4	Loose countera ction
	1	>814	0-32	675.7	1.5-10.4	724.1	1.4-9.5	1298.0	1.4-3.8	Countera ction material
	2	116-430	7-32	261.9	10.4□	290.0	9.5□	489.9	3.8-27.2	Regolith s/colluvi a
	3	16.7-70.0	13-32					1012.4	37.2□	Wet weathere d sandst.
9	0			2956.9	0-0.9	2877.1	0-1.1	2969.9	0-1.2	Loose countera

									ction
1	>814	0-14	998.6	0.9-10.3	817.2	1.1-9.6	1142.4	1.2-4.8	Counteraction material
2	116-430	2.5-27	56.8	10.3	40.4	9.6	663.2	4.8-10.7	Regoliths/colluvia
3	16.7-70.0	2.5-35					41.7	10.7	Wet weathered sandst.

The first units in the VES were not revealed in the ERI models due to their lager minimum electrode spacing of 10 m. Generally, the ERI and VES compared reasonably in mapped structures, resistivity and depth trend in the controls and landslide profiles (Table 7). The slight differences in mapped depth structures between the methods could be attributed to the vertical and lateral resistivity mapping with ERI as against only vertical resistivity mapping with VES and points misalignment during data acquisition.

4.2.5 Comparison of Geophysical and Laboratory Results

The ERI and VES geophysical control results revealed the lithologies as silty clay (16.7 – 70 Ωm), clayey sand (116 – 430 Ωm) and sandstone (>814 Ωm). The landslide profile, however, mapped the counteraction material, regoliths/colluvia and wet weathered sandstone structures. The regoliths/colluvia consist of slumped silty clay silty, sandy clay, silty sandy clay and building relics. The laboratory analysis landslide revealed the dominantly existed in-situ lithologies as silty sandy clay brown silty clay, brown, sandy silty clay and reddish brown sandstone.

4.2.6 Environmental, Engineering and Groundwater Implications

The control profile revealed well layered lithologies of silty clay (16.7 – 70 Ωm), clayey sand (116 – 430 Ωm) and sandstone (>814 Ωm). The underlying sandstones resistivity reflected a non-weathered and protective layer to shallow aquifer. The mapped sandstones in the landslide site showed various degree of weathering and wetting with resistivity value range of 16.7 - 70.0 Ωm. The overlying regoliths and colluvia, following the in-situ silty clay, clayey silty sand lithologies slump, lost their matrix cementation, creating more liquid infiltration path down the underlying sandstone and exposing the shallow aquifers to contamination. This agrees to Egbueri and Igwe (2018) that Ogwashi formation underlying the study areas are characterized by numerous surface water bodies and shallow groundwater systems. Both the surface waters and groundwater have a westward flow direction, from areas of high elevations on the Nanka formation to areas of

low elevations on the Ogwashi formation and the soils are permeable, weak, easily dispersible and collapsible. The landslide site being high gully slope gradients collect large volume of floods during intense rainy season. The floods wash the standing lithologies and infiltrates into the underlying sandstone leading to its weathering. This leads to more unstability of the easily dispersible and collapsible engineering soils and exposes adjoining buildings to danger as observed on the site.

5.0 Conclusions

In an attempt to address the devastating effect of Uruagu landslide in Nnewi North LGA of Anambra State, the deployed geoelecrical methods successfully unraveled the landslide soil failure mechanisms. The findings revealed three in-situ strata for the ERI and VES with different grades of cohesive soil (silt and clay) composition with variations in resistivity signatures. The landslide site, however, revealed three disorderedly layered strata for the ERI and three – four strata for VES. The laboratory analysis of the landslide sites revealed the dominantly existed in-situ lithologies as silty sandy clay, silty clay, sandy silty clay and sandstone, collaborating the ERI and VES control profiles (in-situ). The first layer (topsoil) in the landslide is the counteraction material. This structure comprises laterites, conglomerates and boulders of different rocks as observed physically on the sites. The counteraction material which varies in thickness across the sites serves as some fillings across the concave sloppy depression. The second unit is the regoliths and colluvia. They include the intercalations of slumped in-situ silty clay, silty sandy clay, sandy silty clay and clayey silty sand units of the site as derived from the laboratory analysis. The structure has undergone some diagenesis leading to it being more permeable, weak, easily dispersible and collapsible, following the uneven badland topography, high gully slope gradients, concave slopes. The sandstone unit forms the third layer. It is characterized with low resistivity signatures. The low resistivity values result from wetting of the soil matrix due to strong mechanical stresses during the landslide occurrence leading to water infiltration from the overlying regoliths and colluvia. The sandstone surface is the gliding/sliding surface the overlying units slump or creep during failure. The VES revealed same resistivity signature in collaboration to the landslide ERI. However, the slight differences in mapped depth structures between the ERI and VES methods could be attributed to the vertical and lateral resistivity mapping with ERI as against only vertical resistivity mapping with VES.

The laboratory textural description of the two landslide sites revealed silty sandy clay, silty clay, sandy silty clay and sandstones as the dominantly pre-landslide existing lithologies in no stratification order. The dominantly cohesive soils, (silty sandy clay, silty clay and sandy silty clay) in the sites,

from the plasticity chart, belong to the inorganic clays of medium plasticity and are classified as highly plastic. These soils during intense rainfall, imbibe more water, following their high plasticity, slid along the sandstone to activate the landside. The geophysical and laboratory results revealed consistency in the lithological units in agreement to the characteristic geology of the study area. The landslide sites have high gully slope gradients and collect large volume of floods during intense rainy season. The floods wash the standing lithologies and infiltrates into the underlying sandstone leading to its weathering. This leads to more unstability of the easily dispersible and collapsible engineering soils and exposes adjoining buildings to danger as observed on the sites.

6.0 References:

1. **Ayolabi, E. A.,** Folorunso, A. F. and Jegede, O. E. (2013). An Application of 2D Electrical Resistivity Tomography in Geotechnical Investigation of Foundation Defects: A Case Study. *Journal of Geology and Mining Research.* Vol. 3 (2); 142-151.
2. **Bisdorf, R.J** and Lucius, J.E (1999**).** Mapping the Norman-Oklahoma Landfill Contaminant Plume Using Electrical Geophysics. *U.S Geological Survey Water Resources Investigation Report,* **6**: 99-401
3. **Bogoslovsky, V. A**. and Ogilvy, A. A. (1977). Geophysical methods for the investigation of landslides. *Geophysics*, vol. 42, no. 3, Pp. 562–571. Doi:10.1190/1.1440727
4. **Casagrande, A**. (1932). "Research of Atterberg Limits of Soils," Public Roads, Vol. 13 (8): 121–136.
5. **Chikwelu, E. E**. and Chetty, N. (2021). Use of Electrical Resistivity Tomography in investigating the internalStructure of a landslide and its groundwater characterization (Nanka Landslide, Anambra State, Nigeria). Journal of Applied Science and Engineering, Vol. 25, No 4, Page 763-772 dx.doi.org/10.6180/jase.202208_25(4).0012
6. **Coduto, D.P**. (1999**).** *Geotechnical Engineering: Principles and Practice*. Upper Saddle River Prentice Hall Inc
7. **Cruden, D.M** and Varnes, D.J. (1996). Landslide types and processes. Special Report – National Research Council, Transportation Research Board. Vol 247, pp. 36-75.
8. **Dahlin, L.T**., Forsberg, K., Nilsson, A. and Flyhammer, P. (2006). Resistivity Imaging for Mapping of Groundwater Contamination at the Municipal Landfill La Chureca, Managua, Nicaragua. Near Surface 2006, 12th European Meeting of Environmental and Engineering Geophysics, 4–6 September, Helsinki, Finland

9. **Daily, W.** and Ramirez, A.L. (2000). Electrical imaging of engineered hydraulic barriers. *Geophysics*, 65(1), pp.83 – 94.
10. **Egbueri, J. C.** and Igwe, O. (2021). The impact of hydrogeomorphological characteristics on gullying processes in erosion-prone geological units in parts of southeast Nigeria. Geology, Ecology, and Landscapes **5**(3): 227–240. DOI: 10.1080/24749508.2020.1711637.
11. **Evrett ME**. 2013. Near-surface Applied Geophysics.Cambridge: Cambridge University Press.
12. **Ezemonye, M.N**., and Emeribe, C.N. (2012). Rainfall erosivity in southeastern Nigeria. Ethiopian Journal of Environmental Studies and Management 5 (2): 112–122.
13. **Igwe, O.,** Mode, W., Nnebedum, O., Okonkwo, I. and Oha, I. (2013). The analysis of rainfall-induced slope failures at Iva Valley area of Enugu state, Nigeria. Environment and Earth Science. https://doi.org/10.1007/s12665-013-2647
14. **Igwe, O.** and Una, C.O. (2019). Landslide impacts and management in Nanka area, Southeast Nigeria. *Geoenvironmental Disaster*. 6(5), pp 1-12.
15. **Kearey, P.,** Brooks, M. and Hill, I. (2002). An Introduction to Geophysical Exploration.3rd edition- Blackwell Science Ltd, Oxford, pp 262.
16. **Loke, M.H**. (2001). Electrical Imaging Survey for environmental and engineering studies: A practical guide for 2D and 3D surveys. www.geoelectrical.com p.62
17. **Merritt, A.J.**, Chambers, J.E., Murphy, W. et al.(2013). 3D ground model development for an active landslide in Lias mudrocks using geophysical, remote sensing and geotechnical methods, Landslides, vol 11, no. 4, pp. 537-550. DOI 10.1007/s10346-013-0409-1
18. **McCann, D.M**, Forster A (1990) Reconnaissance geophysical methods in landslide
19. investigations. Eng Geol 29:59–78
20. **Monanu, S.,** and Inyang, F. (1975). Climatic regimes. In Nigeria in Maps (ed. by, ed. G.E.K. Ofomata, 27–29. Benin: Ethiope Publ. House.
21. **Nfor, B N;** Olobaniyi, S B; Ogala, J E (2007). Extent and distribution of groundwater resources in parts of Anambra State, Southeastern, Nigeria. Journal of Appl. Sci. Environ. Manage. vol. 11 (2) 215 - 221
22. **Nigeria Meteorological Agency (NIMET)** (2007). Daily weather forecast on the Nigerian Television Authority. Nigerian Metrological Agency, Oshodi, Lagos

23. **Nwajide, C.S**. (1980). Eocene tidal sedimentation in the Anambra Basin, southern Nigeria. Sedimentary Geology 25: 189–207.
24. **Onyekwelu, C. C**. Onwubuariri, C. N. Mgbeojedo, T. I. Al□Naimi, L. S. Ijeh, B. I. Agoha, C. C.(2021) Geo□electrical investigation of the groundwater potential of Ogidi and environs, Anambra State, South□eastern Nigeria. Journal of Petroleum Exploration and Production Technology. doi.org/10.1007/s13202-021-01119-z
25. **Pazzi, V**.; Morelli, S. and Fanti, R (2019). A review of the advantages and limitations of geophysical investigations in landslide studies. *International Journal of Geophysics.* v. 2019, pp 27
26. **Perrone**, **A**., Lapenna, V. and Piscitelli, S.(2014).Electrical resistivity tomography technique for landslide investigation: a review. *Earth-Science Reviews*, vol. 135, pp. 65–82.
27. **Rezaei, S.;** Shooshpasha, I.; Rezaei, H. (2019). Reconstruction of landslide model from ERT, geotechnical, and field data, Nargeschal landslide, Iran. *Bulletin of Engineering Geology and the Environment* , v. 78, n.5, p. 3223-3237,.
28. **Sechman, H**., Mościcki, W.J. and Dzieniewicz, M. (2013). Pollution of near-surface zone in the vicinity of gas wells. *Geoderma*, 197–198, pp. 193 – 204
29. **Uwaezuoke, C.C.,** Ishola, K.S. & Ayolabi, E. A. (2021) Electrical resistivity imaging and multichannel analysis of surface waves for mapping the subsurface of a Wetland Area of Lagos, Nigeria, NRIAG Journal of Astronomy and Geophysics, 10:1, 300-319, DOI:10.1080/20909977.2021.1927427
30. **Whiteman, A (1982)** Nigeria: Its petroleum geology, resources and potentials, vol 1. Graham &Trotman, Londonpressures in the Anambra basin, southern Nigeria. Hydrol Sci J 42(2):141–154